Mon. Not. R. Astron. Soc. **336,** 527–540 (2002)

The effect of cooling and preheating on the X-ray properties of clusters of galaxies

Orrarujee Muanwong,[1]★ Peter A. Thomas,[1] Scott T. Kay[1] and Frazer R. Pearce[2]

[1]*Astronomy Centre, CPES, University of Sussex, Falmer, Brighton BN1 9QJ*
[2]*Physics and Astronomy Department, University of Nottingham, Nottingham NG7 2RD*

Accepted 2002 June 10. Received 2002 June 7; in original form 2002 May 10

ABSTRACT

We calculate X-ray properties of present-day galaxy clusters from hydrodynamical cosmological simulations of the ΛCDM cosmology and compare these with recent X-ray observations. Results from three simulations are presented, each of which uses the same initial conditions: *Non-radiative*, a standard adiabatic, non-radiative model; *Radiative*, a radiative model that includes radiative cooling of the gas; and *Preheating*, a preheating model that also includes cooling but in addition impulsively heats the gas prior to cluster formation. At the end of the simulations, the global cooled baryon fractions in the latter two runs are 15 and 0.4 per cent, respectively, which bracket the recent result from the *K*-band luminosity function. We construct cluster catalogues that consist of over 500 clusters and are complete in mass down to $1.18 \times 10^{13}\, h^{-1}\, \mathrm{M}_{\odot}$. While clusters in the *Non-radiative* simulation behave in accord with the self-similar picture, those of the other two simulations reproduce key aspects of the observed X-ray properties: namely, the core entropy, temperature–mass and luminosity–temperature relations are all in good agreement with recent observations. This agreement stems primarily from an increase in entropy with respect to the *Non-radiative* clusters. Although the physics affecting the intracluster medium is very different in the latter two models, the resulting cluster entropy profiles are very similar.

Key words: hydrodynamics – methods: *N*-body simulations – galaxies: clusters: general – intergalactic medium – X-rays: galaxies: clusters.

1 INTRODUCTION

Because of numerical limitations, most previous simulations of clusters of galaxies have been adiabatic, resulting in approximate self-similar scaling for cluster properties. However, these models are unphysical in that the cooling time of the gas in the central regions of the clusters is less than their age; also, observed clusters do not scale self-similarly. In this paper, we generate mock cluster catalogues from simulations that include radiative cooling, and we show that these can reproduce the observed scaling relations.

The observed X-ray luminosity–temperature (L_{X}–T_{X}) relation has a slope as large as 3 (e.g. Edge & Stewart 1991), steeper than the predicted value of 2 from self-similarity. Cooling flows, which are known to exist in a large population of clusters (Allen & Fabian 1998), are one cause of this, as the more massive, cooling flow clusters have an excess of luminosity. However, when the cooling flow components are corrected for, the observed slopes are still significantly larger than 2 (Allen & Fabian 1998; Markevitch 1998). The departure from self-similarity is even more prominent in low-mass clusters or groups (Ponman et al. 1996; Xue & Wu 2000) where the slope can be as steep as 8. These departures from self-similarity can help us to learn about the history of the intracluster medium (ICM).

The L_{X}–T_{X} relation predicted from self-similarity, when bremsstrahlung is assumed to dominate the emission, can be written as $L_{\mathrm{X}} \propto f_{\mathrm{gas}}^2 (1+z_{\mathrm{form}})^{3/2} T^2$ where f_{gas} is the gas mass fraction and z_{form} is the formation redshift. Mohr, Mathiesen & Evrard (1999) and Arnaud & Evrard (1999) present evidence that the intracluster medium is more extended in low-mass clusters so that f_{gas} is a mildly increasing function of temperature, but the latter also stress that this is statistically inconclusive because their sample is not homogeneous and the results are model-dependent.

One explanation for the above observations is that galaxy formation is more efficient in poor groups than clusters. David et al. (1990) show that the ratio between the gas and stellar mass increases with gas temperature. They argue that, as mergers take place to form massive clusters, the gas is heated and this suppresses galaxy formation. Bryan (2000) compiled observed mass fractions in groups and clusters from various studies. By assuming variations of galaxy formation efficiencies and applying them to a simple model, he successfully predicted the L_{X}–T_{X} relation. This motivates our *Radiative* simulation in which gas is removed from the ICM by radiative cooling. We are somewhat fortunate in that the finite resolution of the

★E-mail: O.Muanwong@sussex.ac.uk

simulation limits the amount of cooling (or else the vast majority of the gas would have cooled to low temperatures) and leads to a similar amount of star formation as Bryan suggests is required to reproduce the observations.

Kaiser (1991) and Evrard & Henry (1991) suggest an alternative way of expelling gas from clusters via energy injection at early times, perhaps feedback from galaxy formation. The gas does not have to be removed from the cluster entirely but only from the central regions that dominate the X-ray emission. Observational evidence is provided by Ponman, Cannon & Navarro (1999) who show that the surface brightness profiles of cool and hot systems are not scaled versions of each other and that the core entropies of low-temperature clusters are higher than can be achieved by gravitational collapse alone. It appears that the core entropy approaches a certain value, approximately 100 $h^{-1/3}$ keV cm^2, at low temperature that they designate the 'entropy floor'.

For this preheating model to work, it has to happen in an optimal way, i.e. the right amount of energy has to be injected at the right time. There have been various studies which suggest that, if an energy is injected well before cluster collapse, 0.3 keV per particle is required (Lloyd-Davies, Ponman & Cannon 2000). If energy injection takes place internally, i.e. within collapsed haloes, more energy is required, 1–3 keV per particle (Lowenstein 2000; Wu, Fabian & Nulsen 2000; Bower et al. 2001). The efficiency of energy injection depends on the density of the intergalactic medium (IGM): the higher the density, the more energy is required to achieve the same entropy level. These results motivate our *Preheating* simulation in which, in addition to radiative cooling, the gas is preheated by raising the specific energy by 1.5 keV at a redshift of 4.

It has been shown that there is a need for some form of feedback energy into the ICM in order to get a suitable cooled baryon fraction (White & Frenk 1991; Cole 1991; Blanchard, Valls-Gabaud & Mamon 1992). Without such a process, too much gas would be cooled and converted into stars at high redshift. As haloes at high redshift are small and dense, cooling becomes very efficient. A vast fraction of gas is cooled into small systems, leaving only a small amount of hot gas in the haloes to form galaxies at later times, the so-called 'cooling catastrophe' (White 1992). The picture of this process is clearly in contradiction with observations as large amounts of hot baryons are observed in X-ray clusters at the present day.

Unfortunately, an accurate determination of the cooled gas fraction in clusters of galaxies is hard to obtain. From recent observations of the *K*-band luminosity function, Balogh et al. (2001) show that the global cooled baryon fraction is only about 5 per cent. Using a sample of clusters compiled by Roussel, Sadat & Blanchard (2000) and Carlberg et al. (1996), they estimated a cooled fraction of around 20 per cent for systems with $kT = 1$ keV, decreasing to around 10 per cent at $kT = 10$ keV. Note, however, that these results rely on extrapolating the observations out to the virial radii (by as much as a factor of 5 in radius for low-temperature systems). These observations do not preclude excess cool material in a form other than stars, such as neutral or molecular gas. Indeed, the models of Bryan (2000) and Wu & Xue (2002b) both required a cooled gas fraction in clusters of about twice the above in order to reproduce the X-ray scaling relations.

Despite this uncertainty in the cooled gas fraction in real clusters, our *Radiative* and *Preheating* simulations are likely to bracket the true value. We will show below that in all other respects the clusters in our simulations reproduce the X-ray properties of clusters extremely well. This agreement stems from the entropy profiles, which are similar in the two simulations and much shallower than in a *Non-radiative* simulation.

In Section 2, we describe the simulations and explain how we construct our simulated cluster catalogues. The properties of the ICM are presented in Section 3, and the temperature–mass and luminosity–temperature scaling relations are discussed in Section 4. Finally we summarize our conclusions in Section 5.

2 METHODOLOGY

2.1 Simulation details

Simulation data were generated using a parallel implementation of the HYDRA code (Couchman, Thomas & Pearce 1995; Pearce & Couchman 1997), which uses the adaptive particle–particle/particle–mesh (AP^{3}M) algorithm to calculate gravitational forces (Couchman 1991) and smoothed particle hydrodynamics (SPH) to model hydrodynamical forces. Our implementation of SPH is similar to that used by and discussed in Thacker & Couchman (2001).

Results are presented assuming a flat, low-density cosmology, setting the density parameter $\Omega_0 = 0.35$, Hubble constant $h = 0.71$,[1] cosmological constant $\Omega_\Lambda = \Lambda/3H_0^2 = 0.65$, baryon density $\Omega_b = 0.019\,h^{-2}$, cold dark matter power spectrum shape parameter $\Gamma = 0.21$ and normalization $\sigma_8 = 0.9$. The initial density field was realized by perturbing 4096 000 (160^3) particles each of dark matter and gas from a regular cubic mesh of comoving length, 100 h^{-1} Mpc. Thus, dark matter and gas particle masses are approximately $2.1 \times 10^{10}\,h^{-1}\,M_\odot$ and $2.6 \times 10^9\,h^{-1}\,M_\odot$ respectively. Each simulation was then evolved to $z = 0$, typically taking around 2000 steps, using 64 processors on the Cray T3E at the Edinburgh Parallel Computing Centre. The gravitational softening length was fixed at $\epsilon = 50\,h^{-1}$ kpc in comoving coordinates (equivalent Plummer value) until $z = 1$, after which it was fixed in physical coordinates at $\epsilon = 25\,h^{-1}$ kpc until $z = 0$. This choice prohibited unwanted relaxation effects (see below).

In this paper we study three simulations that differ only in the manner in which the gas particles are cooled and heated:

Non-radiative. This simulation does not contain any radiative cooling, and heating occurs solely by adiabatic compression and shock heating. As discussed previously (Thomas et al. 2001, hereafter T2001; Muanwong et al. 2001, hereafter M2001), this run does not provide an accurate physical description of clusters since gas with short cooling times cannot cool, but it serves as a useful model for comparison and to test numerical effects.

Radiative. In this simulation the gas was allowed to cool radiatively, using cooling tables from Sutherland & Dopita (1993). We adopted a global gas metallicity of $Z = 0.3(t/t_0)\,Z_\odot$, where t/t_0 is cosmic time in units of the present value. Material that had cooled (identified as all gas particles with overdensities $\delta > 1000$ and temperatures $T < 1.2 \times 10^4$ K) was identified on each step, and groups of 13 particles within a softening length were merged into single collisionless particles (hereafter referred to as 'galaxy fragments'). Fragments could subsequently accrete more cooled gas (within a softening length) but not merge with other fragments. We do not discuss the properties of these galaxy fragments in this paper.

Preheating. This is identical to the *Radiative* run, except that all gas particles were impulsively heated by adding 1.5 keV of thermal energy at $z = 4$, corresponding to an increase in temperature of approximately 1.2×10^7 K.

[1] We define $h = H_0/100$ km s^{-1} Mpc^{-1}.

As we shall see, both the *Radiative* and *Preheating* runs reproduce the observed cluster scaling relations but contain vastly different amounts of cooled gas.

2.2 Cluster identification

In this paper, we present results only for clusters at $z = 0$.[2] Clusters are identified using an identical procedure to that used by M2001, as described below.

First, we create a minimal spanning tree of all dark matter particles whose density exceeds 317 times the mean dark matter density in the box. (For a spherical top-hat model, this is equal to the mean density within virialized regions, although the precise density used does not matter at this stage.) We then define a maximum linking length equal to $0.5(317)^{-1/3}$ times the mean interparticle separation and use this to split the minimal spanning tree into clumps of particles that serve as potential sites of clusters. The centre of each clump is defined as the position of the densest dark matter particle; then a sphere is grown around all particles until radii are found that enclose average overdensities of 111 (i.e. $317\Omega_0$), 200, 500, 1000 and 2500 relative to the critical density, $\rho_{\rm cr} = 3H_0^2/8\pi G$. Clumps are written into the cluster catalogues provided that they contain a mass equivalent to at least 500 particles each of gas and dark matter within these radii, and that their centres are not located within a more massive cluster.

As we are interested in the X-ray properties of clusters, we did consider using gas particles rather than dark matter particles to define the cluster centre. However, we decided against this for two reasons: first, in runs with radiative cooling the densest gas particle was often located in the outskirts of the cluster as defined by the dark matter; secondly, it made it hard to compare clusters from different simulations that had similar dark matter distributions but very different gas ones.

The catalogues are complete in mass down to $1.18 \times 10^{13}\, h^{-1}\, {\rm M}_\odot$. Our final catalogues for each simulation have of the order of 530, 460, 350, 250 and 150 clusters within the overdensities mentioned above, respectively. Although we do not report on them in this paper, we have also created cluster catalogues for a large number of higher redshifts, and all the catalogues are available on-line.[3]

2.3 Numerical heating

When undertaking an N-body simulation, it is crucial to use an appropriate gravitational softening length (see, for example, T2001). Ours is chosen following the Thomas & Couchman (1992) criterion such that the smallest clusters in all simulations presented here have two-body relaxation times of at least five times the age of the Universe. Also, for a metallicity $Z = 0$, the mass of each dark matter particle is approximately equal to the critical mass, as estimated by Steinmetz & White (1997), above which there would be enough spurious numerical heating to suppress cooling within the haloes. This is the most conservative case, since $Z > 0$ when the first resolved haloes form in the simulations.

As a check on the degree of numerical heating in our simulations, we plot in Fig. 1 the ratio of the total specific energy of the gas, $\epsilon_{\rm gas}$, to that of the dark matter, $\epsilon_{\rm dm}$, as a function of mass, $M_{\rm vir}$, contained within the virial radius, $r_{\rm vir}$ (defined as the radius that encloses a mean overdensity of 111 times the critical density, in accord with Section 2.2). The specific energy of the gas consists of the kinetic and thermal contributions of hot gas particles (throughout this paper we use the term 'hot gas' to mean gas particles with temperatures in excess of 10^5 K) with masses m_i, speeds v_i (relative to the cluster mean) and temperatures T_i:

$$\epsilon_{\rm gas} = \frac{\sum_i m_i \left(\frac{1}{2}v_i^2 + 3kT_i/2\mu m_{\rm H}\right)}{\sum_i m_i}, \qquad (1)$$

where $\mu m_{\rm H}$ is the mean molecular mass, which we take to be 10^{-24} g for a cosmic mix of elements. (Note that we assume the ratio of specific heats, $\gamma = 5/3$, corresponding to a monatomic ideal gas.) The specific energy of the dark matter particles can similarly be written as

$$\epsilon_{\rm dm} = \frac{\sum_i \frac{1}{2} m_i v_i^2}{\sum_i m_i}. \qquad (2)$$

In the *Non-radiative* simulation, the ratio of specific energies (top panel of Fig. 1) is independent of cluster mass. The outliers that have the highest and lowest values of the energy ratio in the figures are subclumps that are falling into large neighbouring clusters. We illustrate this by using solid triangles to denote clusters where the mean relative velocity of the gas and dark matter is more than 0.1 times

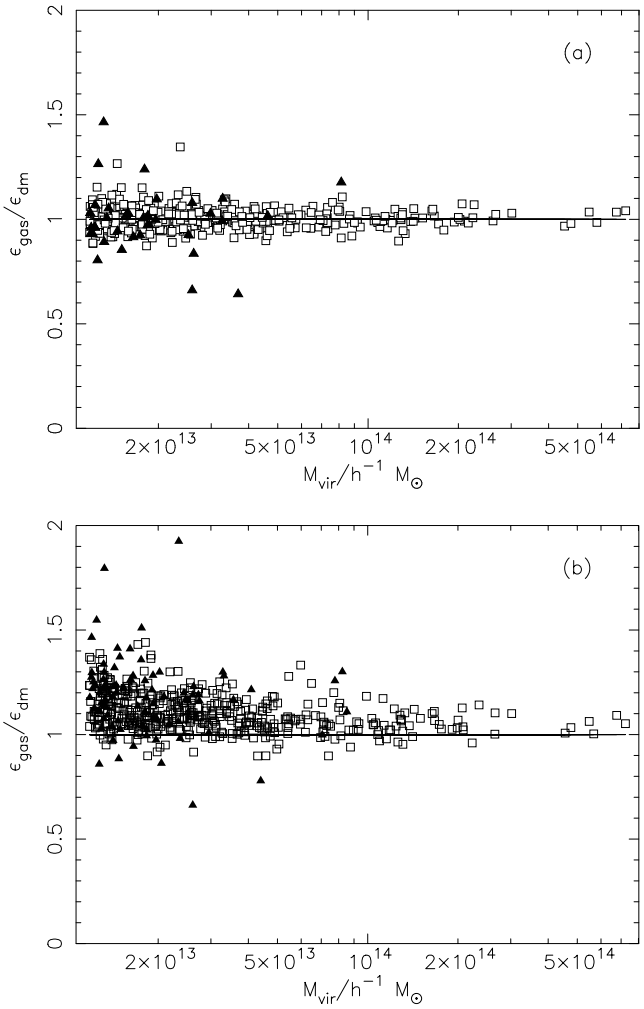

Figure 1. Ratios between the specific energy of the gas and the dark matter within the virial radii of clusters in the (a) *Non-radiative* and (b) *Radiative* simulations. The filled triangles correspond to clusters that show significant velocity substructure, as described in the text.

[2] For clarity, we choose not to discriminate between groups and clusters, and use only the latter term.

[3] http://virgo.sussex.ac.uk/

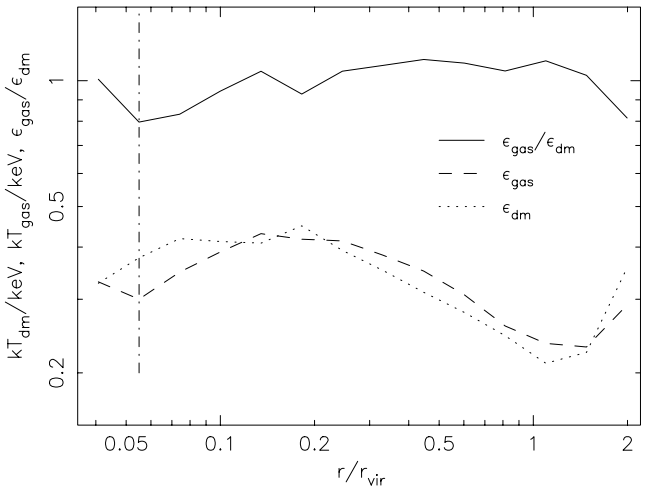

Figure 2. Averaged profiles of specific energy of the gas, $\epsilon_{\rm gas}$, and the dark matter, $\epsilon_{\rm dm}$, and the ratio between the two, for the 10 least-massive clusters in the *Non-radiative* simulation. The units are defined in the usual manner of X-ray observations in kT units, such that $kT = \frac{2}{3}\mu m_{\rm H}\epsilon$. The vertical line indicates the softening length.

the velocity dispersion of the cluster (and in fact one of the open squares that lie above the mean relation designates a cluster that only just failed this cut). When radiative cooling is included (lower panel), the gas component is found to have a higher specific energy than the dark matter and the ratio increases with decreasing mass; similar results are found for the *Preheating* simulation. This result shows that radiative cooling leads to mass deposition and, paradoxically, a heating of the residual ICM through adiabatic compression, a result first demonstrated in a cosmological simulation by Pearce et al. (2000, although see also Knight & Ponman 1997). In any event, the difference between the two panels shows that physical heating processes overwhelm numerical ones in our simulations.

To test our results further, we show in Fig. 2 average energy profiles for the 10 smallest clusters in the *Non-radiative* simulation. The specific energies of the gas and dark matter follow each other well at all radii and show no evidence for an increase in gas specific energy over that of the dark matter near the centres of the clusters.

3 PROPERTIES OF THE INTRACLUSTER MEDIUM

3.1 Baryon fractions

In this section, we look at the relative distribution of baryons and dark matter in the simulated clusters. Fig. 3(a) shows the baryon fraction within the virial radius, in units of the global baryon fraction, for the *Non-radiative* simulation. Note that, even for the largest clusters in our catalogues, the ICM is more extended than the dark matter. This is because, for a given specific energy (see Fig. 1), the gas is better able to support itself in the gravitational potential than the dark matter. The effect is more pronounced in smaller clusters, although this may be an artefact of poorer resolution in these objects.

In the *Radiative* run (Fig. 3b), the total baryon fraction in the clusters is almost unchanged. However, the mass fraction of hot gas (i.e. the hot intracluster medium that gives rise to X-ray emission) is much reduced, especially in the low-mass clusters. The *Preheating* run (Fig. 3c) also reduces the hot gas fraction in the centres of clusters, but it does so by a different mechanism. Instead of turning hot

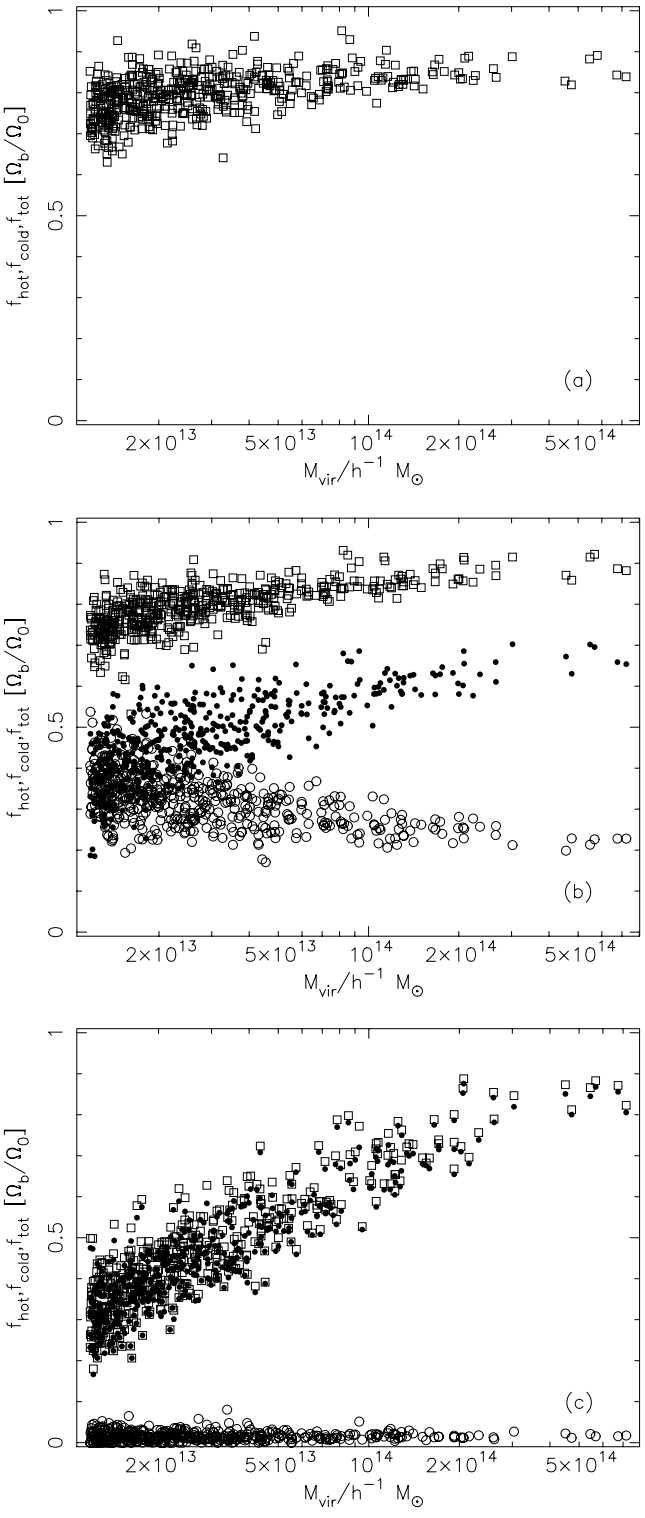

Figure 3. Mass fractions of hot gas (solid circles), cold gas (open circles) and the total fractions (squares) within the virial radius of clusters in the (a) *Non-radiative*, (b) *Radiative* and (c) *Preheating* simulations.

gas into cooled gas (which term we take to include stars and galaxies), it heats it up and expels it from the cluster core. In low-mass clusters, the gas is expelled from the cluster altogether, resulting in a reduced baryon fraction within the virial radius, whereas in high-mass clusters it is merely redistributed to larger radii but remains within the cluster.

Neither the *Radiative* nor the *Preheating* runs give the correct fraction of cooled gas. The global cooled fraction in the box is 15 per cent for the former and 0.4 per cent for the latter. However, we will show later that the X-ray properties of the clusters from the two simulations are very similar because they both have similar entropy profiles. Only when we look at the outer parts of clusters can the two be easily distinguished.

3.2 The entropy of intracluster gas

For a given gravitational potential, the spatial distribution of the ICM in hydrostatic equilibrium is determined by its entropy (plus one normalization condition such as the pressure at, or the total mass within, the virial radius). Higher entropies correspond to more extended gas distributions, and, in particular, a high core entropy leads to a reduction in the gas density near the centre of the cluster and hence a much reduced X-ray luminosity.

In this paper, we follow the usual practice in observational X-ray papers and work not with entropy but with the closely related quantity

$$s_{\rm X}(r) = \frac{kT_{\rm X}(r)}{n_{\rm e}(r)^{2/3}}, \tag{3}$$

where $n_{\rm e}$ is the electron density and $T_{\rm X}$ is the emission-weighted X-ray temperature,

$$T_{\rm X} = \frac{\sum_i m_i \rho_i \Lambda_{\rm soft}(T_i, Z) T_i}{\sum_i m_i \rho_i \Lambda_{\rm soft}(T_i, Z)}. \tag{4}$$

Here m_i, ρ_i and T_i are the mass, density and temperature of the hot gas particles that contribute to the X-ray emission, Z is the metallicity, and $\Lambda_{\rm soft}$ is the cooling function from Raymond & Smith (1977) in the soft band, 0.3–1.5 keV. (For a fully ionized plasma with a cosmic distribution of helium, then $n_{\rm e} \approx 0.88\rho/m_{\rm H}$.)

In the absence of radiative cooling, the entropy of the gas can only increase through shock heating associated with mergers and accretion. Within any given cluster, there will be a range of entropies, with a positive entropy gradient from the centre outwards (this comes about both because shock heating is more effective for material accreted later and because any other distribution is convectively unstable). For a self-similar cluster population for which we measure $s_{\rm X}$ at some fixed fraction of the virial radius (and hence the same value of $n_{\rm e}$ for each), then $s_{\rm X} \propto T_{\rm X}$. In a real cluster population this proportionality will not be exact because the profiles are not exactly self-similar [the 'concentration' varies with mass (see e.g. Navarro, Frenk & White 1997; T2001)], but it will nevertheless hold to good approximation.

However, this self-similarity does not seem to extend down to low-mass clusters and groups. Ponman et al. (1999) and Lloyd-Davies et al. (2000) found that, when measuring the entropy at a fiducial radius of $0.1r_{\rm vir}$, which they termed the 'core entropy', hot clusters appeared to follow the prediction from self-similarity whereas cool clusters lay above it. (We note that the term 'core entropy' does not imply that clusters show a constant entropy in the innermost regions – they do not. It is used as a loose term to define the entropy outside the central cooling region but still near the centre of the cluster.) Although the observations are not very precise, a rough interpretation is that the core entropy flattens off and approaches a constant value, termed the 'entropy floor', in small systems. Ponman et al. (1996) attributed this effect to preheating of the intergalactic medium before cluster formation (and thus motivated the *Preheating* model in this paper).

In this section, we calculate the core entropy of our clusters in a similar way as in the above observations. We average the value of $s_{\rm X}$ in a spherical annulus centred on $0.1r_{\rm vir}$ and of width $\Delta r = 0.02r_{\rm vir}$ (there are various other ways of doing this averaging, but they all give similar results). We note that $0.1r_{\rm vir}$ is about twice the softening length for the smallest clusters in our catalogues.

The core entropies of the clusters in the three simulations are plotted against their X-ray temperatures in Fig. 4. Also shown is an approximate fit to the observed relation from Ponman et al. (1999, solid curves) and the prediction from the non-radiative numerical simulations of Eke, Navarro & Frenk (1998, dashed lines). In the *Non-radiative* run (Fig. 4a), the core entropy follows the self-similar relation well, albeit with large scatter. On the other hand, the core entropies of clusters in the *Radiative* and *Preheating* simulations (Figs 4b and c, respectively) are in good agreement with the observations (solid curves). In the *Preheating* simulation, the excess entropy relative to the self-similar prediction is due to the increase in energy of the gas at $z = 4$ (given that radiative losses in this simulation are negligible, the excess entropy is conserved). The agreement of the *Radiative* simulation with observations, however, is somewhat fortuitous: in the absence of some form of feedback mechanism, the amount of gas that cools to low temperatures is determined only by the resolution of the simulation and the imposed metallicity of the gas.

3.3 Entropy and temperature profiles

Fig. 5 shows entropy profiles for high- and low-mass clusters from each simulation. The entropy is defined as in equation (3) except that we use the mass-weighted rather than the emission-weighted temperature. The high-mass cluster is the third largest in the box and was chosen because the two most-massive clusters show significant amounts of substructure within their virial radii; even for this cluster, however, there is an obvious subclump at about $0.7r_{\rm vir}$ that significantly distorts the entropy profile in the *Non-radiative* simulation. The low-mass profiles were constructed by averaging the profiles of the 10 lowest-mass clusters in each simulation that did not show significant substructure – only about half the clusters were deemed acceptable. Thus neither panel is representative of a typical cluster in our simulations as most have much more substructure than is visible here.

First note that the entropy profiles of the three runs roughly match for the massive cluster at radii greater than $0.3r_{\rm vir}$. The differences are due to different amounts of cool gas in subclumps that permeate the outer regions of all clusters. Within this radius, the *Radiative* and *Preheating* runs have significantly higher entropy than the *Non-radiative* one. For the *Preheating* run, this excess entropy arises from the energy injection at $z = 4$ and is subsequently almost unchanged, except for a slight decrease within $0.04r_{\rm vir}$, where radiative cooling has had a small effect. The entropy increase in the *Radiative* simulation, although it follows that in the *Preheating* run closely, comes about through an entirely different mechanism, namely inflow of high-entropy gas to replace low-entropy gas lost via cooling. That the two agree is coincidental except inasmuch as we have chosen the simulation parameters such that the two runs have similar X-ray properties.

For the low-mass clusters the behaviour is similar, except that the excess entropy extends out to a larger fraction of the virial radius. The *Radiative* and *Non-radiative* runs have converged by $r = 2r_{\rm vir}$ since cooling is efficient only in the centre of the cluster. In the *Preheating* run, however, the excess entropy is still apparent beyond $2r_{\rm vir}$ as the entropy was increased for all of the gas.

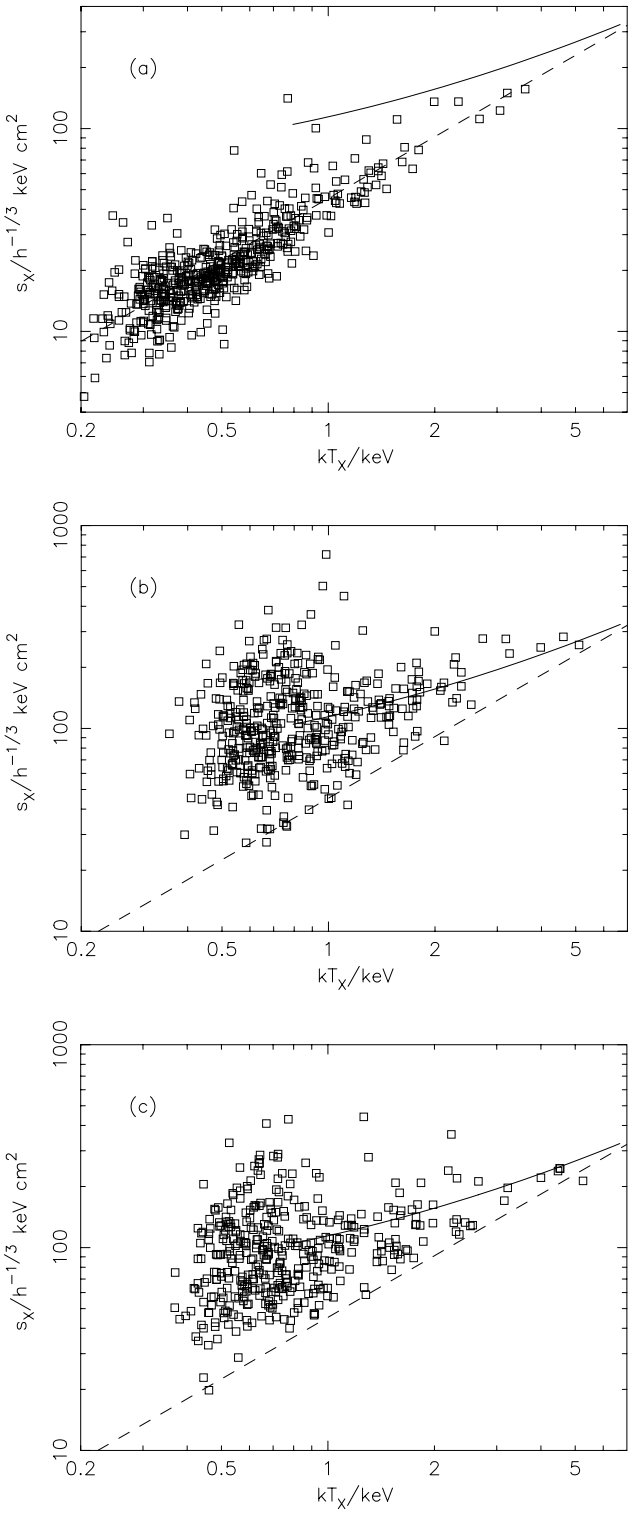

Figure 4. Core entropy at $0.1r_{\rm vir}$ versus X-ray temperature for clusters in the (a) *Non-radiative*, (b) *Radiative*, and (c) *Preheating* simulations. The straight dashed line is the self-similar relationship from the simulations of Eke et al. (1998). The solid curve is an approximate fit to the Ponman et al. (1999) data points from their fig. 2.

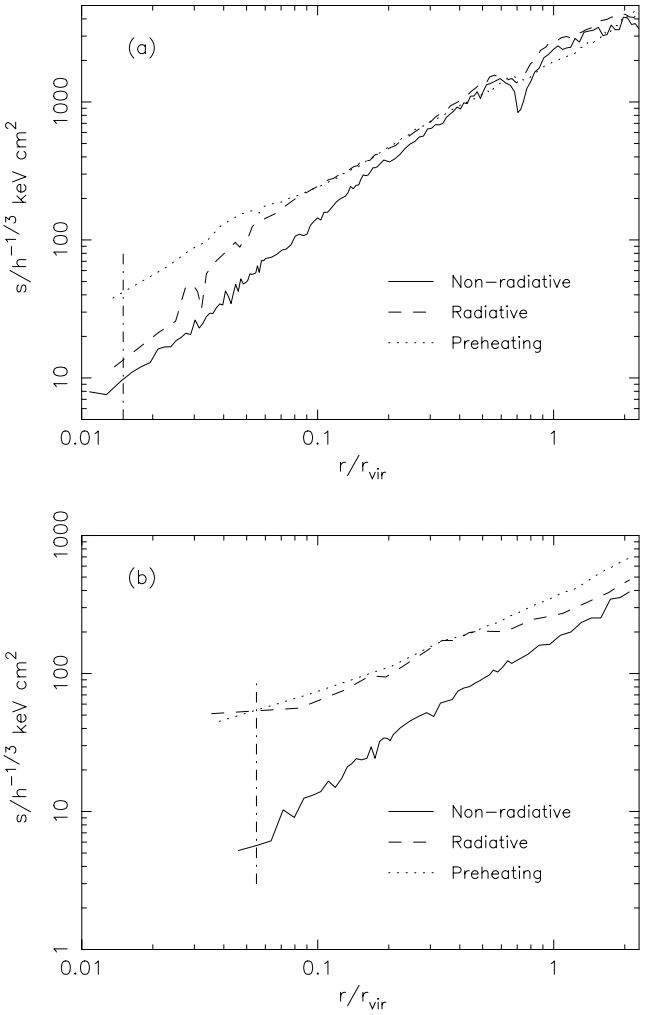

Figure 5. The entropy profiles in each of the three simulations of (a) the third most-massive and (b) the 10 least-massive clusters that did not show significant substructure. The long dash-dotted line indicates the gravitational softening length. Bins were chosen so as to average over at least 32 particles near the cluster core, with more further out.

For all clusters in the *Preheating* simulation, the excess entropy is much less than expected for gas at the mean density of the box at the time of preheating (about 770 $h^{-1/3}$ keV cm^2). This is because the intracluster gas at $z = 0$ was already in overdense structures by $z = 4$. For example, the average density of the gas in the 10 least-massive clusters is about 20 times the mean gas density at $z = 4$. Thus, the additional energy injected into the gas only increased the entropy by approximately 100 $h^{-1/3}$ keV cm^2, as is evident from Fig. 5.

Fig. 6 shows mass-weighted temperature profiles for the same clusters as in Fig. 5. Emission-weighted temperatures are similar to these in the inner parts of clusters but decline more rapidly in their outer regions owing to the presence of dense, cool subclumps. Note that the excess temperature in the intracluster medium in the *Preheating* simulation is much less than 1 keV/k, except near the cores of the largest clusters. Thus, the gas must have cooled adiabatically, flowing out of clusters and reducing its density, since the time it was heated. By contrast, the gas in the *Radiative* run has flowed inwards, raising its temperature by adiabatic compression.

In their inner regions, the clusters are approximately isothermal. However, the gas temperature declines rapidly at large radii, typically dropping by a factor of 2–3 from its peak out to the virial radius, in agreement with results from previous simulations (e.g. Frenk et al. 1999). Recent observational evidence finds no evidence

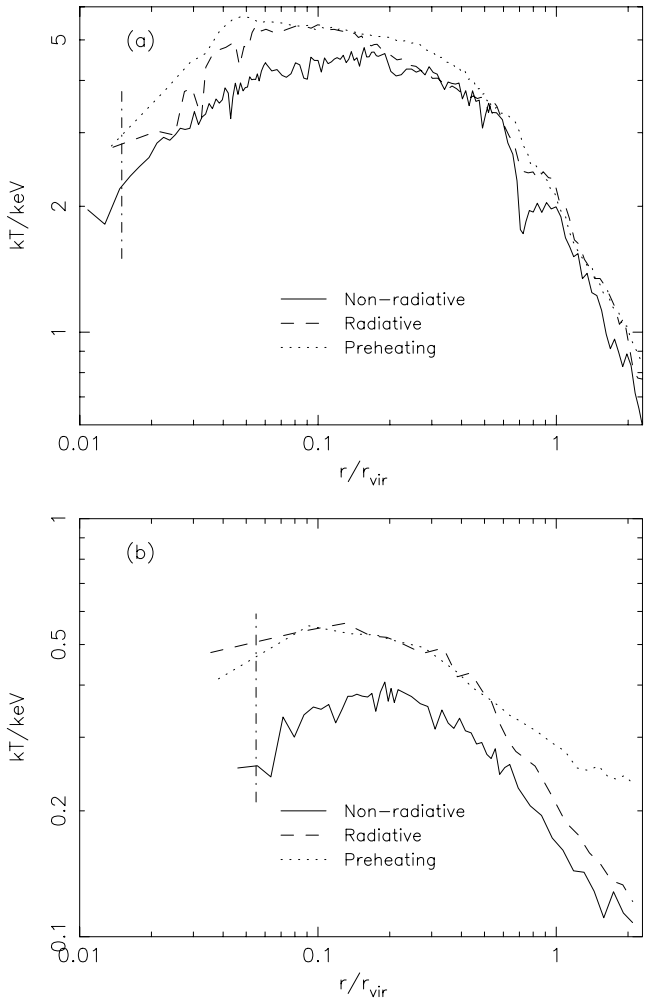

Figure 6. The mass-weighted temperature profiles of (a) the third most-massive and (b) the 10 least-massive clusters that did not show significant substructure. The long dash-dotted line indicates the gravitational softening length. Bins were chosen so as to average over at least 32 particles near the cluster core, with more further out.

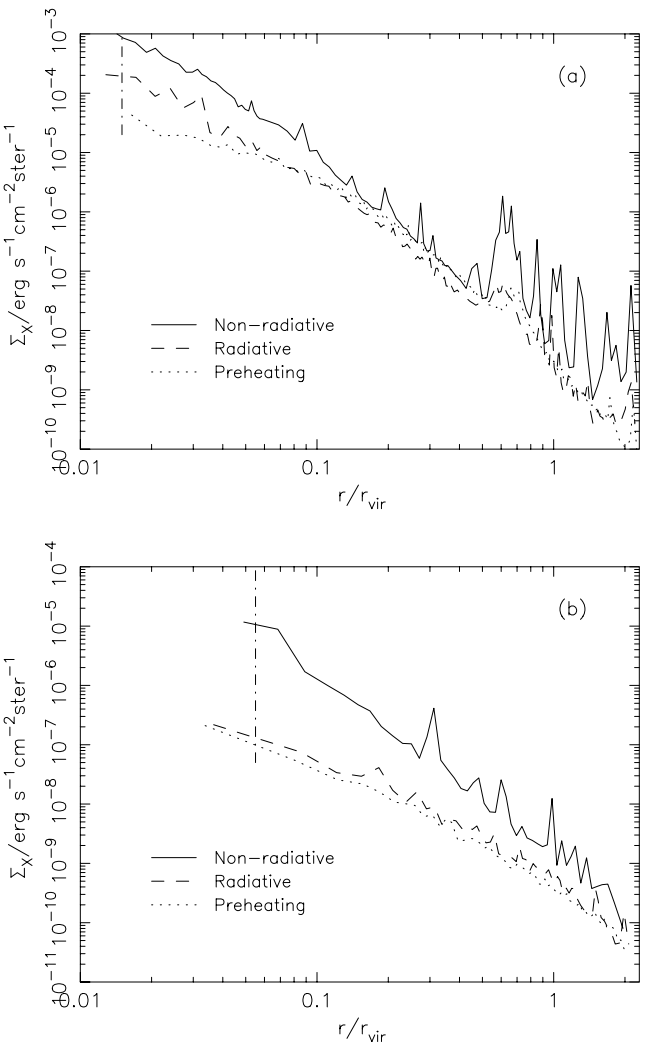

Figure 7. The averaged X-ray surface brightness profiles in the 0.3–1.5 keV band in each of the three simulations of (a) the third most-massive and (b) the 10 least-massive clusters that did not show significant substructure. The long dash-dotted line indicates the gravitational softening length. Bins were chosen so as to average over at least 64 particles near the cluster core, with more further out.

of departures from isothermality of X-ray clusters (Irwin, Bregman & Evrard 1999; White 2000; see, however, Markevitch 1998) but only probe out to about $0.4r_{\rm vir}$, just where the temperature profiles steepen. If these observations can be extended out to larger radii, then this would be a strong test of the models.

3.4 Surface brightness profiles

X-ray surface brightness profiles for the third most-massive cluster and an averaged low-mass cluster are shown in Fig. 7. Note, once again, the significant substructure that is present even in these profiles that have been specially selected to be as smooth as possible. This substructure is particularly prevalent in the X-ray surface brightness because of its weighting with the square of the gas density.

The total masses in the intracluster medium within the virial radius of the massive cluster in the *Preheating* and *Non-radiative* simulations are roughly equal, yet the *Non-radiative* simulation has a higher surface brightness at all radii – this is because of emission from high-density gas in subclumps that is heated and expelled in the *Preheating* run.

The isothermal-β model (Cavaliere & Fusco-Femiano 1976) is commonly used to estimate cluster masses. The model assumes a halo to be a spherical, isothermal sphere. The surface brightness profile of an isothermal gas in hydrostatic equilibrium within such a halo is

$$\Sigma_{\rm X}(R) = \Sigma_{\rm X}(0)[1 + (R/R_{\rm c})^2]^{1/2-3\beta_{\rm fit}}, \qquad (5)$$

where $R_{\rm c}$ is the X-ray core radius. It is not at all obvious that equation (5) provides a good description of the surface brightness profiles in real clusters. These often fail to flatten in their inner regions as much as is predicted by equation (5), so the central regions are then omitted from the fitting and the excess emission over the isothermal-β model is attributed to a cooling flow. Furthermore, the outer radius to which one can measure the surface brightness accurately is only a small fraction of the virial radius and depends upon the size and distance of the cluster.

We now estimate the values of $\beta_{\rm fit}$ for our simulated clusters. Then later, in Section 4.1, we will test the reliability of cluster masses deduced using the isothermal-β model. An accurate comparison

with X-ray observations would require us to produce mock X-ray data from our simulations, with appropriate particle backgrounds, etc., and then to run these through the X-ray analysis software. We do not yet have the tools to do this, so instead adopt a simpler procedure that is robust even in the presence of substructure. As seen in Fig. 7, the surface brightness profiles of the simulated clusters fluctuate, even well within the virial radius. In order to smooth the profiles, we integrate them inwards to obtain a cumulative luminosity profile. Using the isothermal-β model, this can be expressed as

$$L_{\rm X}(>R) = L_{\rm X}(0)[1 + (R/R_{\rm c})^2]^{3/2-3\beta_{\rm fit}}, \quad (6)$$

where R denotes a two-dimensional, projected radius. We need a statistic that is insensitive to emission from the outer parts of clusters (where most of the substructure originates) and from a possible central cooling flow. One such is

$$\mathcal{L} = \frac{L_{\rm X}(>R_{\rm mid}) - L_{\rm X}(>R_{\rm out})}{L_{\rm X}(>R_{\rm in}) - L_{\rm X}(>R_{\rm out})}, \quad (7)$$

which depends only on the flux between $R_{\rm in}$ and $R_{\rm out}$, where $R_{\rm in} < R_{\rm mid} < R_{\rm out}$.

In our fits, we fix $R_{\rm out} = 0.4r_{200}$, which is approximately equal to the outer extent of observed X-ray surface brightness profiles. We also fix $R_{\rm in} = R_{\rm c} = R_{\rm KS}$, where $R_{\rm KS}$ is based on the model of Komatsu & Seljak (2001). They determined a relationship between the core radius of the X-ray emission and the concentration parameter of the dark matter density profile (Navarro et al. 1997),

$$R_{\rm KS} \approx 0.4r_{500}/c, \quad (8)$$

where

$$c = 6\left(\frac{M_{\rm vir}}{10^{14}\,h^{-1}\,{\rm M}_\odot}\right)^{-1/5}. \quad (9)$$

[We note that Komatsu & Seljak (2001) inadvertently put the factor of 0.4 above into the denominator rather than the numerator in equation (8); the expression as we give it is compatible with their fig. 13.] Finally, we take $R_{\rm mid} = 0.15r_{200}$ and then solve equations (6) and (7) for $\beta_{\rm fit}$ with the results shown in Fig. 8.

The first thing to note is the scatter in the calculated values of $\beta_{\rm fit}$. This is because individual surface brightness profiles are very noisy as a result of the presence of substructure. Secondly, there is a trend for the mean value of $\beta_{\rm fit}$ to decrease with decreasing temperature in the *Radiative* and *Preheating* simulations with the value of approximately 2/3 in large clusters. The trend is much less apparent in the *Non-radiative* model where most clusters throughout the temperature range have consistently high values of $\beta_{\rm fit}$. Komatsu & Seljak (2001) propose that such a trend may arise from observational bias due to the fact that one observes out to a larger fraction of the virial radius in higher-mass clusters; that is not the explanation here, as we have fixed $R_{\rm out} = 0.4R_{200}$ (we tried taking a variable outer radius as described by Komatsu & Seljak, but found that it made little difference to our results). Rather, the difference in $\beta_{\rm fit}$ values between the *Non-radiative* and the other two runs is a real one, reflecting the raised entropy and hence the reduced density in the inner regions of low-mass clusters in the *Radiative* and *Preheating* runs.

If the data were of sufficiently high quality, one could evaluate $\mathcal{L}$ at two different choices of $R_{\rm mid}$ and then solve for both $R_{\rm c}$ and $\beta_{\rm fit}$. In practice, there is a strong correlation between these two parameters, and the solutions sometimes return unacceptably large values of $R_{\rm c}$ (greater than $R_{\rm out}$) and correspondingly large values of $\beta_{\rm fit}$. It is for this reason that we fix the core radius before fitting. Fortunately, $\beta_{\rm fit}$ is insensitive to the precise choice of core radius: we have checked that doubling the value of the core radius, i.e. setting $R_{\rm c} = 2R_{\rm KS}$, does not alter the results significantly. We have also taken the more conventional approach of fitting functions of the form of equation (5) directly to the surface brightness profiles. This again gives similar results but with larger scatter. This is because the surface brightness fitting is more sensitive to the presence of substructure at the outer edge of the fit than is the method that we describe above.

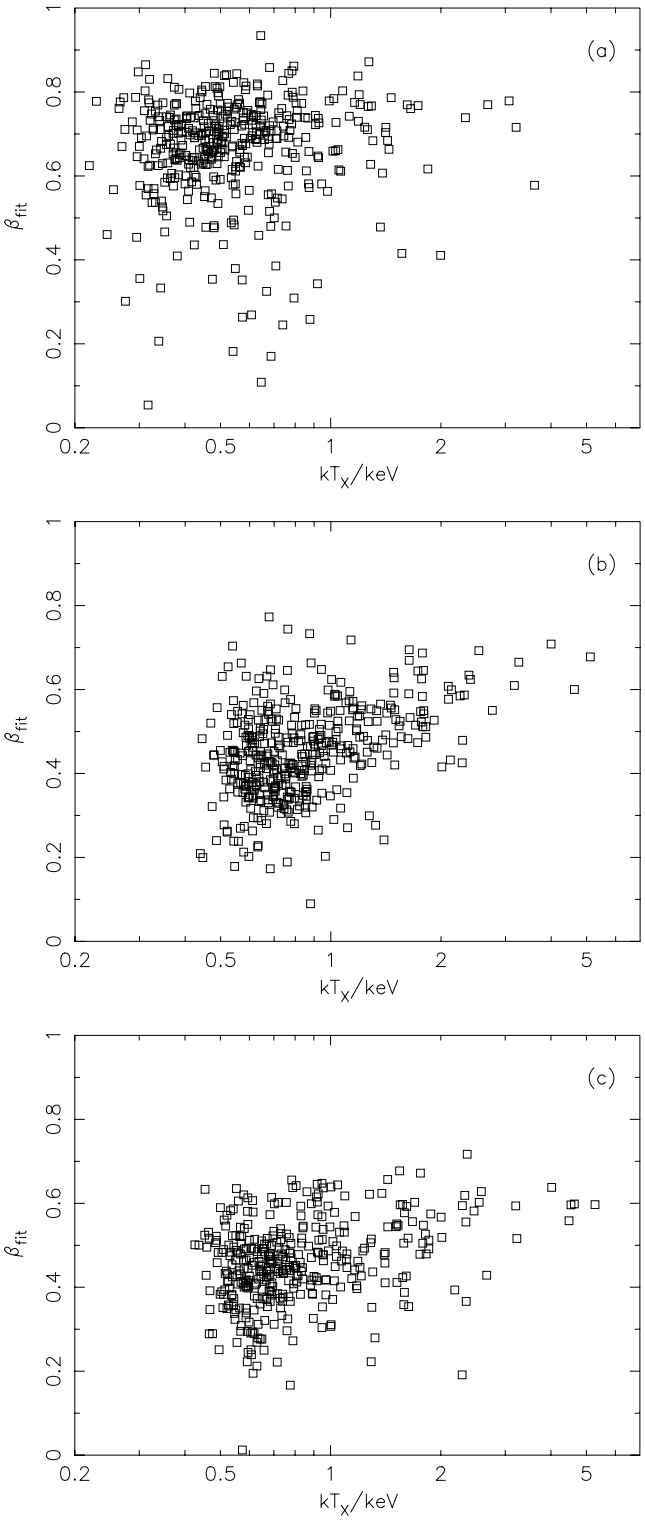

Figure 8. The surface brightness fitting parameter, $\beta_{\rm fit}$, as a function of temperature in the 0.3–1.5 keV band, for clusters drawn from the (a) *Non-radiative*, (b) *Radiative* and (c) *Preheating* simulations.

The measurement of the $\beta_{\rm fit}$ parameter as presented above is far removed from the usual observational practice. Nevertheless, we shall see in Section 4.1 that the total mass within r_{200} when determined using the parameter is in good agreement with observations.

3.5 Cooling flows

There is currently considerable confusion over the observational evidence for cooling flows in clusters of galaxies. Recent results show not only a deficit of soft X-ray emission lines (e.g. Peterson et al. 2002) but also evidence for low-temperature gas at approximately 10^5 K (Oegerle et al. 2001) and even large amounts of molecular gas (Edge 2001). Our simulations do not have the resolution to investigate cooling flows in detail. Here we simply wish to test whether the standard method of calculating mass deposition rates gives the correct answer.

In this section, we calculate mass deposition rates using two methods: (i) by directly measuring the rate at which gas cools out of the hot intracluster medium to temperatures below 10^5 K, and (ii) by measuring the emission from within the cooling radius, defined as the radius within which the gas has a mean cooling time less than 6 Gyr.

Fig. 9 illustrates the two measures of the mass deposition rate for clusters in the *Radiative* and *Preheating* simulations. The solid circles show the actual mass deposition rate averaged over the last few output times in our simulations, corresponding to a time interval of just under 1 Gyr. Although the mass is measured in $h^{-1}\,{\rm M}_\odot$, we have plotted it in units of $h^{-2}\,{\rm M}_\odot\ {\rm yr}^{-1}$ to aid comparison with the predicted rate. The particle resolution limits the measurement of the mass deposition rate to be a multiple of approximately $3\,h^{-2}\,{\rm M}_\odot\ {\rm yr}^{-1}$. Note that the mass deposition is extremely stochastic in that the mass deposition rate in the first half of this time interval typically differs from that in the second half by a factor of more than 2.

The open squares show the predicted mass deposition rate, defined as

$$\dot{M}_{\rm pred} = \frac{L_{{\rm X},r_{\rm cool}}}{5kT_{{\rm X},r_{\rm cool}}/2\mu m_{\rm H}}, \qquad (10)$$

where $L_{{\rm X},r_{\rm cool}}$ and $T_{{\rm X},r_{\rm cool}}$ are the bolometric luminosity and mean temperature within the cooling radius within which the gas has a mean cooling time of less than 6 Gyr. The temperature and luminosity here are estimated from emission in the soft band, as described in equations (4) and (14). Although there is a large scatter, the predicted and actual mass deposition rates roughly agree, with no evidence of a systematic bias of one above the other. Because of uncertainties in the definition of the predicted cooling rate, one should not make too much of this agreement. Nevertheless, it does eliminate the possibility, within the context of the models that we simulate, that incorrect interpretation of the X-ray observations has led to a vast overestimate of the actual mass deposition rate in clusters.

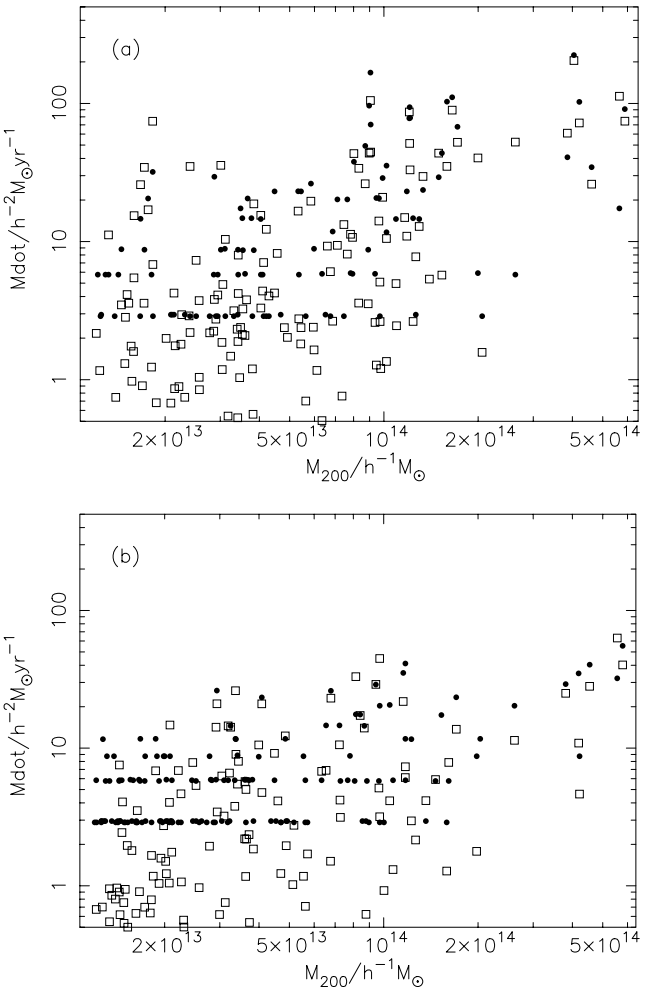

Figure 9. The mass deposition rates for clusters drawn from the (a) *Radiative* and (b) *Preheating* simulations. The open squares show the predicted mass deposition rate based on the soft-band X-ray emission from within the cooling radius; the solid circles show the actual mass deposition rate averaged over approximately 1 Gyr.

4 SCALING RELATIONS

4.1 Temperature–mass relation

The most direct way to compare the simulated temperature–mass[4] relation between simulated and observed clusters is to use the thermal (mass-weighted) temperature of the gas within a small region that is well observed in X-rays. We have already done this and presented the results in a short paper (Thomas et al. 2002), in which we compared the simulations described in this paper with observations of five relaxed clusters using the *Chandra* satellite (Allen, Schmidt & Fabian 2001). In particular, we compared the normalization of the temperature–mass relation for matter within r_{2500} (where r_Δ is the radius of the sphere that encloses a mean density of Δ times the critical density). The *Non-radiative* simulation agrees with previous simulations of that kind (e.g. Mathiesen & Evrard 2001) in predicting temperatures that are too low for a given mass, whereas both the *Radiative* and *Preheating* simulations reproduce the observations. Unfortunately, spatially resolved temperature data are as yet available only for a few bright clusters, and so the overlap in mass between the observed and simulated clusters is small; nevertheless, there is no reason to expect that our simulated results should not extend up to higher temperatures.

A much larger body of data exists for emission-weighted temperatures of clusters, with poor spatial resolution. In this case some form of modelling is required in order to derive the mass. The emission-weighted temperature, being dominated by the high surface brightness, central regions of the clusters, does not change very much with

[4] We use temperature–mass rather than mass–temperature because we are complete in mass rather than temperature.

r_Δ, but the mass does. Generally, one wants to choose as small a radius as possible in order to minimize the extrapolation outside the region that is well observed in X-rays. On the other hand, theoretical predictions are for the mass within the virial radius ($\Delta = 111$ in this cosmology). In this paper, we compromise and use $\Delta = 200$, as this is the overdensity used in two observational papers with which we wish to compare: Horner, Mushotzky & Scharf (1999) and Xu, Jin & Wu (2001). A third (Finoguenov, Reiprich & Böhringer 2001) uses $\Delta = 500$ but is easily extrapolated to $\Delta = 200$ (using $M \propto \Delta^{-1/2}$ for the isothermal-β model at radii much greater than the core radius).

kT_X–M_{200} relations for the clusters are presented in Fig. 10. We use the cooling table of Raymond & Smith (1977) to calculate the X-ray temperature in the soft band (0.3–1.5 keV), as described in Section 4. The open squares show the temperature calculated using all the particles in the clusters. However, the presence of cold, high-density gas in the cluster cores (and also in infalling subclumps) gives emission-weighted temperatures that are well below the virial temperature of the cluster. Accordingly, we also show as filled circles, for the *Radiative* and *Preheating* runs, the 'cooling-flow-corrected temperature' obtained by omitting emission from within the cooling radius, as defined in Section 3.5. The change is most important for high-mass clusters, for which it has the effect of both tightening the relation and bringing it closer to the predicted slope of 2/3. The cooling flow correction does not work very well for clusters in the *Non-radiative* simulation, which have cool, dense gas at all radii: for this run, therefore, we show instead the effect of omitting all gas particles with cooling times shorter than 6 Gyr.

Most of our clusters are smaller than those for which X-ray masses have been determined. Hence, to facilitate comparison with observations, we fitted a power law to the temperature–mass relation for clusters more massive than $5 \times 10^{13}\, h^{-1}\, \mathrm{M}_\odot$. Table 1 lists the normalization, A, and slope, α of the relation

$$kT_X = A\left[M_{200}/\left(3 \times 10^{14}\, h^{-1}\, \mathrm{M}_\odot\right)\right]^{1/\alpha} \mathrm{keV}, \qquad (11)$$

where we have chosen to normalize at a mass scale of $3 \times 10^{14}\, h^{-1}\, \mathrm{M}_\odot$ – towards the upper end of our simulated catalogue but the lower end of most observed ones.

We have divided Table 1 into three parts. In the first, we list results from previous simulations: EMN96 – Evrard, Metzler & Navarro (1996); BN98 – Bryan & Norman (1998); T2001 – Thomas et al. (2001); ME01 – Mathiesen & Evrard (2001). These use various cosmologies, but fortunately the results do not seem to be very sensitive to this. Much more important is the resolution of the simulation. Thus ME01 have higher resolution than previous simulations (unfortunately they do not state their precise mass resolution in the paper) and find a lower normalization; our current simulations have a higher resolution again and lower the normalization still further. The reason why the increasing resolution lowers the emission-weighted temperature of the gas is the presence of cold, dense gas in subclumps. When we exclude gas with a cooling time of less than 6 Gyr from the calculation, then we find that the emission-weighted temperature rises once more to a similar value to that found in the earlier, low-resolution simulations.

The middle section of Table 1 shows results for the clusters described in the current paper for emission in the soft band, 0.3–1.5 keV, both with and without the inclusion of gas within the cooling radius. The cooling flow correction has little effect on clusters in the *Non-radiative* simulation, mainly because of the presence of cool gas in infalling subclumps (the effect of removing all gas with

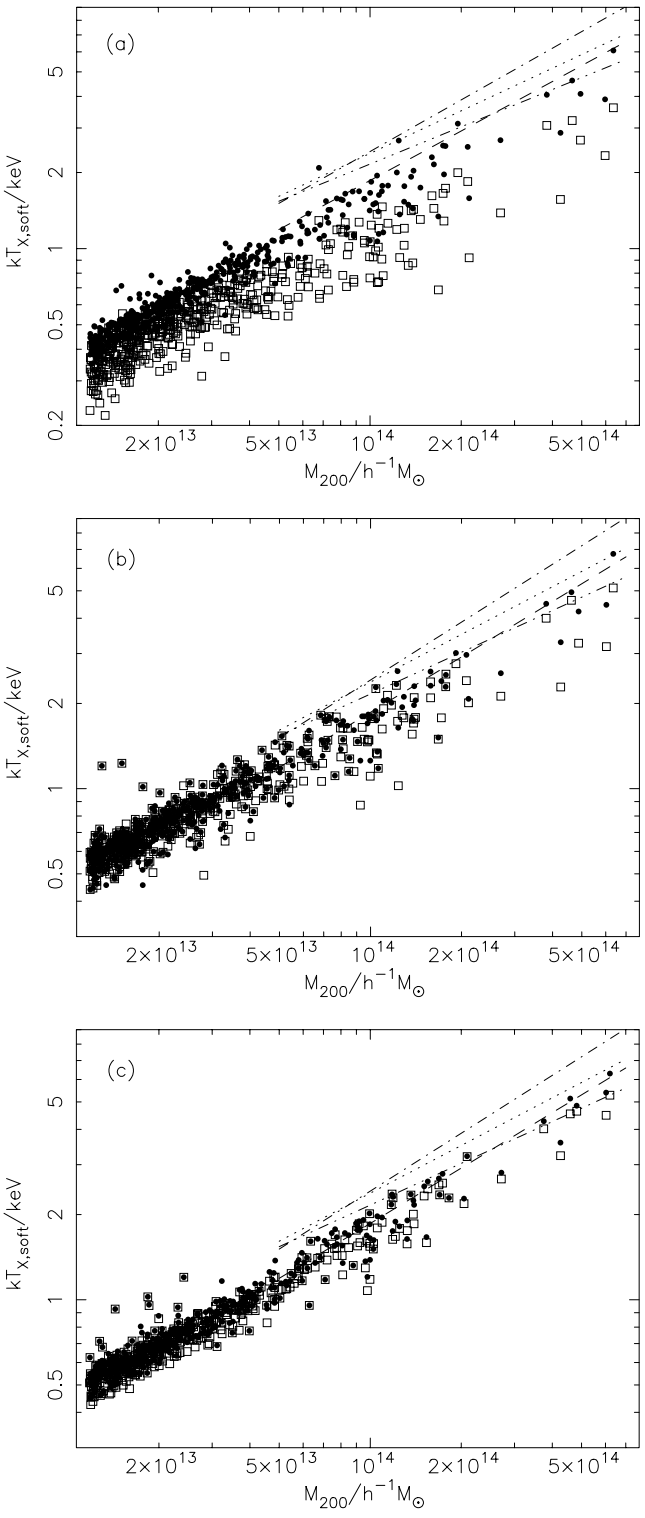

Figure 10. The X-ray temperature versus mass relation for the (a) *Non-radiative*, (b) *Radiative* and (c) *Preheating* simulations. The open squares show the total soft-band X-ray temperature, whereas the filled circles exclude emission from (a) gas with short cooling times, or (b, c) gas within the cooling radius. The different lines are from observations (Horner et al. 1999) using mass estimates from galaxy velocity dispersions (dashed line), X-ray temperature profiles (dot-dashed line), the isothermal-β model (dotted line), and emissivity profiles derived by surface brightness deprojection (triple-dot-dashed line).

Table 1. Power-law fits to the observational and simulated temperature–mass relations of X-ray clusters: cluster sample; slope of relation, α; value of kT/keV at $3 \times 10^{14}\, h^{-1}\, \mathrm{M}_\odot$, A.

Sample		α	A
EMN96	Soft band	1.50	3.6
BN98	Bolometric	1.50	2.9
T2001	Bolometric	1.50	3.6
ME01	Broad band, high res.	1.51	2.6
Non-radiative	Bolometric	1.50	2.1
	Bolometric, $t_{\rm cool} > 6$ Gyr	1.51	3.3
Non-radiative	Soft band	1.69	2.0
	Cooling flow corrected	1.69	2.2
Radiative	Soft band	1.96	2.8
	Cooling flow corrected	1.64	3.4
Preheating	Soft band	1.67	3.2
	Cooling flow corrected	1.61	3.5
HMS99	Velocity dispersions	1.53	3.8
	Temperature profiles	1.48	5.1
	Emissivity profiles	2.06	3.7
	Isothermal-β model	1.78	4.4
FRB01	Isothermal-β model	1.67	4.1
	Polytropic-β model, low T	1.87	4.3
	Polytropic-β model, high T	1.48	4.4
XJW01	NFW model	1.81	4.9
	Isothermal-β model	1.60	4.3

short cooling times is much larger and was shown in the first part of the table). On the other hand, gas with a short cooling time in the *Radiative* and *Preheating* simulations resides primarily in the cores of large clusters and its omission does significantly raise the emission-weighted temperature. In a previous paper (Pearce et al. 2000), it was shown that radiative cooling *raises* the temperature of the intracluster medium, and we confirm that result. Unfortunately, this is cancelled by the lower temperature obtained by moving to higher resolution, so that the net effect is to give temperature normalizations that are little changed over earlier, non-radiative, low-resolution simulations

In the lower portion of Table 1, we present some observational determinations of cluster temperatures: HMS99 – Horner et al. (1999); FRB01 – Finoguenov et al. (2001); XJW01 – Xu et al. (2001). It is noticeable that various methods provide very different scaling relations, in both normalization and slope. The two methods that provide the best agreement with the simulations are those that combine optical velocity dispersions either with *ASCA* temperatures or with surface-brightness deprojection of *Einstein* data to create emissivity profiles (White, Jones & Forman 1997). Unfortunately, these are the least reliable, as mass estimates from velocity dispersions are prone to projection effects (e.g. van Haarlem, Frenk & White 1997). Also, the deprojection method requires a large extrapolation from $\Delta \approx 2000$ out to $\Delta = 200$. The highest normalization is provided by using resolved temperature profiles. In principle this should be the most accurate method, but as yet the temperature profiles are poorly determined and a high degree of modelling is required. In two papers by Nevalainen, Markevitch & Forman (1999, 2000), for example, the enclosed gas mass fraction in the clusters A401 and A3571 can be seen to be steeply rising at the virial radius, contrary to expectation.

The greatest degree of consensus is given by different authors using the isothermal-β model, which is another way of saying that different groups measure the same relationship between $\beta_{\rm fit}$ and temperature. In this model, the mass profile is

$$M(<r) \approx 1.11 \times 10^{14} \beta_{\rm fit} \frac{kT}{\rm keV} \frac{r^2}{r_{\rm c}^2 + r^2} \left(\frac{r}{h^{-1}\,\mathrm{Mpc}} \right) h^{-1}\,\mathrm{M}_\odot\,, \tag{12}$$

which gives a mass within r_{200} of

$$M_{200} \approx 7.69 \times 10^{13} \left(\frac{\beta_{\rm fit} kT}{\rm keV} \right)^{3/2} \left(\frac{r_{200}^2}{r_{\rm c}^2 + r_{200}^2} \right)^{3/2} h^{-1}\,\mathrm{M}_\odot\,. \tag{13}$$

In most cases $r_{200} \gg r_{\rm c}$, so that the correction term in the above equation for the finite core radius is approximately unity.

The most extensive analysis of this kind was performed by Finoguenov et al. (2001) for the HIFLUGCS (Highest X-ray Flux Galaxy Cluster Sample) from the *ROSAT* All-Sky Survey. They used $\beta_{\rm fit}$ values taken from fits to the *ROSAT* PSPC data and temperatures mostly from *ASCA*. Where information on temperature gradients was available, they generalized the β model to allow a polytropic equation of state, and this gave very similar results. A similar result is found by Xu et al. (2001) using a smaller sample, and by Horner et al. (1999) using *ASCA* data on 38 clusters from Fukazawa (1997). The slopes of the observed temperature–mass relations are slightly steeper than 1.5, reflecting the fact that the measured values of $\beta_{\rm fit}$ are a slowly increasing function of mass, as we found for the simulated clusters in Section 3.4.

To test whether the temperature–mass relation using the isothermal-β model is consistent with the observations, we estimate the masses of the simulated clusters using equation (13) and the values of $\beta_{\rm fit}$ from Section 3.4. The resulting scaling relation, shown in Fig. 11, is fully consistent with the observations. We do not want to overinterpret this result, as the method of determining $\beta_{\rm fit}$ in Section 3.4 is far removed from the analysis that is carried out on real X-ray data. Ideally, one would create mock observations from the simulations and analyse them in the same way, but that is a complex procedure that is beyond the scope of the present paper. Nevertheless, we tentatively conclude that the isothermal-β model underestimates cluster masses and that there is no disagreement between the masses of simulated and real clusters.

4.2 Luminosity–temperature relation

We define the bolometric X-ray luminosity, estimated from emission in the soft band, as

$$L_{\rm X} = \frac{\Lambda_{\rm bol}(T_{\rm X})}{\Lambda_{\rm soft}(T_{\rm X})} \sum_i \frac{m_i \rho_i \Lambda_{\rm soft}(T_i, Z)}{(\mu m_{\rm H})^2}, \tag{14}$$

where $\mu m_{\rm H} = 10^{-24}$ g is the mean molecular mass, $T_{\rm X}$ is the soft-band X-ray temperature as defined in equation (4), and $\Lambda_{\rm bol}$ and $\Lambda_{\rm soft}$ are the bolometric and soft-band cooling functions, respectively.

$L_{\rm X}$ is plotted against $T_{\rm X}$ both with and without emission from within the cooling radius in Fig. 12. We have restricted the temperature ranges to those for which the catalogues are reasonably complete (as judged by looking at the upper locus of the points in Fig. 10). Also shown on the figure are observed relations from Xue & Wu (2000) who provided a compilation of observed X-ray temperatures and luminosities from the literature. Their sample was divided into three subsamples: groups (below 1 keV), clusters (above 1 keV), and the mixture of the two. Their best fit of each category is shown as the dashed, dot-dashed and dotted lines in the figure.

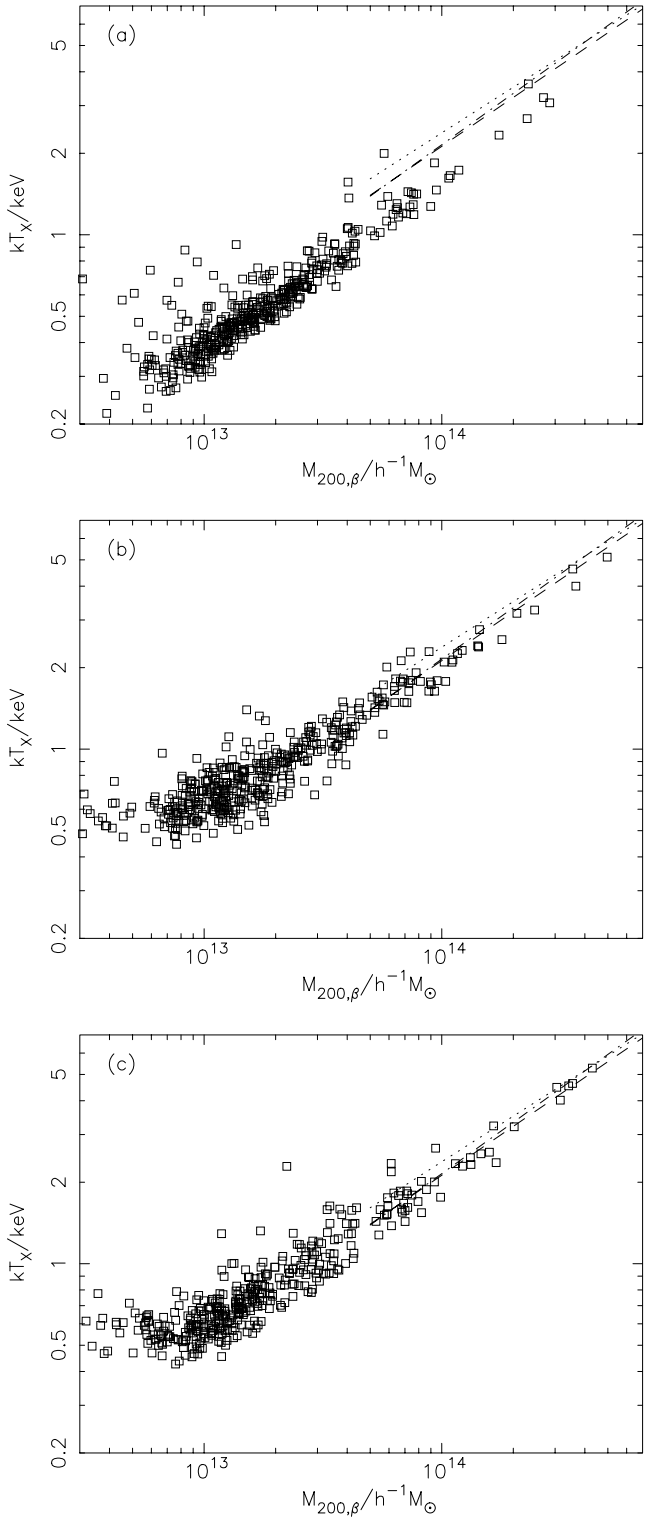

Figure 11. The X-ray temperature versus mass relation for the (a) *Non-radiative*, (b) *Radiative* and (c) *Preheating* simulations, where the mass is estimated from the isothermal-β model. The dotted, dashed and dot-dashed lines are observed masses using isothermal-β model from HMS99, FRB01 and XJW01, respectively.

The first thing to note is that the luminosities of the clusters in the *Non-radiative* simulation are much greater than for observed clusters. These are much reduced, however, by the removal of gas with short cooling times. At temperatures above 1 keV, the uncorrected relation follows the self-similar relation $L_X \propto T_X^2$ expected for bremsstrahlung radiation. At lower temperatures, the luminosity might be expected to exceed the self-similar prediction because of the added flux from line emission, but in fact it is reduced. This is because the cores of the smaller clusters are relatively less well resolved. We do not regard this lack of resolution as important because the gas in the core has a short cooling time and contributes a negligible amount to the total emission in the *Radiative* and *Preheating* simulations.

Both the *Radiative* and *Preheating* simulations show L_X–T_X relations that lie much closer to the observations. The agreement is best for $kT_X > 1$ keV, less so at lower temperatures. This may be because we have not raised the entropy sufficiently in the cores of these systems. However, the observational determination of the X-ray luminosity of low-temperature clusters is very hard (see e.g. Helsdon & Ponman 2000; Wu & Xue 2002a; Voit et al. 2002) and so the lack of agreement is not so serious. For both simulations, but most especially for the *Radiative* one, omission of gas within the cooling radius vastly reduces the scatter and brings the outliers down to the main relation.

5 CONCLUSIONS

We have analysed the properties of clusters drawn from three *N*-body, hydrodynamical simulations of the ΛCDM cosmology. Each uses the same initial conditions but varies in its treatment of the gas physics: a standard adiabatic, *Non-radiative* model; a *Radiative* model that includes radiative cooling of the gas; and a *Preheating* model that also includes cooling but in addition impulsively heats the gas prior to cluster formation. Each simulation generated over 500 clusters, complete in mass down to $1.18 \times 10^{13}\, h^{-1}\, M_\odot$.

The *Non-radiative* simulation does not reproduce the observations but was used as a test of the simulation procedure. The clusters drawn from this simulation show no signs of numerical heating and behave self-similarly in their properties.

Both the *Radiative* and the *Preheating* simulations reproduce three key observational relations:

(i) The entropy in the cores of low-mass clusters lies above the self-similar relation. The measured value at $0.1r_{vir}$ tends towards a value of approximately $100h^{-1/3}$ keV cm^2 at low masses, with very large scatter.

(ii) The luminosity–temperature relations are much reduced in normalization relative to the *Non-radiative* simulation, and lie close to the observed relation above 1 keV once corrected for cooling flow emission. At lower temperatures we still seem to overpredict the X-ray luminosity, although the observational errors are large.

(iii) We have shown in an earlier paper (Thomas et al. 2002) that the temperature–mass relation in the inner parts of clusters, within r_{2500}, agrees with observations. In this paper we reproduce earlier results that show that simulated cluster masses within r_{200} are significantly greater than observed ones for a given cluster temperature. However, we show that the use of the isothermal-β and related models can lead to an underestimate of cluster masses, and once this is taken into account the observations and simulations are once again brought into agreement. The implications of this for the determination of σ_8 from the observed cluster temperature function are the subject of a separate paper, in preparation.

The basic explanation for the agreement in the properties of simulated and observed clusters is an increase in entropy in the cluster cores, over and above that expected in an adiabatic simulation. In the

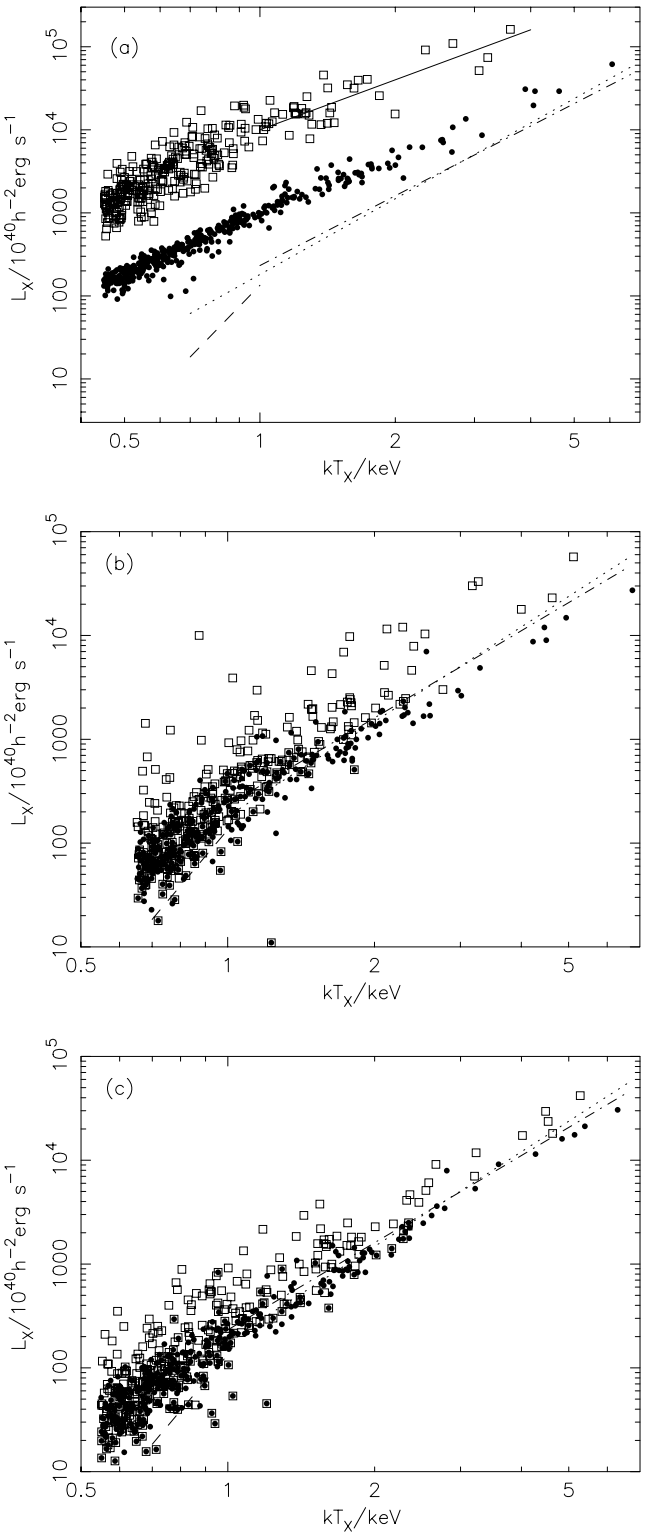

Figure 12. The bolometric X-ray luminosity versus temperature as estimated from the soft band for the (a) *Non-radiative*, (b) *Radiative* and (c) *Preheating* simulations. The open squares use the total soft-band emission, whereas the filled circles exclude emission from (a) gas with short cooling times, or (b, c) gas within the cooling radius. The dashed, dot-dashed and dotted lines are observed relations from Xue & Wu (2000); the solid line in panel (a) shows the self-similar relation $L_X \propto T_X^2$.

Radiative simulation this occurs via the removal of low-entropy gas by radiative cooling, whereas in the *Preheating* simulation it comes about through the imposed energy increase at high redshift. These two mechanisms differ considerably in the amount of cooled gas that results: at the end of the simulations the global cooled baryon fractions are 15 and 0.4 per cent, respectively, bracketing the observed value. Thus, while neither model is a correct description of clusters, one might expect that the true model gives rise to similar entropy profiles.

We showed that the mass deposition rate in cooling flows, i.e. the amount of gas cooling to low temperatures in the cluster cores, is reasonably well approximated by the usual method of dividing the luminosity by the enthalpy within the cooling radius within which the mean cooling time is equal to 6 Gyr. However, the actual mass deposition rate is highly stochastic and may be driven by the infall of high-density subclumps. Higher resolution simulations are required to investigate this further.

In the simulations that we have described in this paper, the cooling is limited by the numerical resolution. Future simulations will move to higher resolution and will have to include the feedback of energy from supernovae. This will act as a form of preheating, thus removing the ad hoc nature of the current model, although it may be that other heating mechanisms are also required. We fully expect that realistic models will emerge that successfully replicate all the observed features of the intracluster medium.

ACKNOWLEDGMENTS

The simulations described in this paper were carried out on the Cray T3E at the Edinburgh Parallel Computing Centre as part of the Virgo Consortium investigations of cosmological structure formation. OM is supported by a DPST Scholarship from the Thai Government; PAT is a PPARC Lecturer Fellow.

REFERENCES

Allen S. W., Fabian A. C., 1998, MNRAS, 297, L57
Allen S. W., Schmidt R. S., Fabian A. C., 2001, MNRAS, 328, L37
Arnaud M., Evrard A. E., 1999, MNRAS, 305, 631
Balogh M. L., Pearce F. R., Bower R. G., Kay S. T., 2001, MNRAS, 326, 1228
Blanchard A., Valls-Gabaud D., Mamon G. A., 1992, A&A, 264, 365
Bower R. G., Benson A. J., Lacey C. G., Baugh C. M., Cole S., Frenk C. S., 2001, MNRAS, 325, 497
Bryan G. L., 2000, ApJ, 544, L1
Bryan G. L., Norman M. L., 1998, ApJ, 495, 80 (BN98)
Carlberg R. G., Yee H. K. C., Ellingson E., Abraham R., Gravel P., Morris S., Pritchet C. J., 1996, ApJ, 462, 32
Cavaliere A., Fusco-Femiano R., 1976, A&A, 49, 137
Cole S., 1991, ApJ, 367, 45
Couchman H. M. P., 1991, ApJ, 368, L23
Couchman H. M. P., Thomas P. A., Pearce F. R., 1995, ApJ, 452, 797
David L. P., Arnaud K. A., Forman W., Jones C., 1990, ApJ, 356, 32
Edge A. C., 2001, MNRAS, 328, 762
Edge A. C., Stewart G. C., 1991, MNRAS, 252, 414
Eke V. R., Navarro J. F., Frenk C. S., 1998, ApJ, 503, 569
Evrard A. E., Henry J. P., 1991, ApJ, 383, 95
Evrard A. E., Metzler C. A., Navarro J. F., 1996, ApJ, 469, 494 (EMN96)
Finoguenov A., Reiprich T. H., Böhringer H., 2001, A&A, 368, 749 (FRB01)
Frenk C. S. et al., 1999, ApJ, 525, 554
Fukazawa Y., 1997, PhD thesis, Univ. Tokyo

Helsdon S. F., Ponman T. J., 2000, MNRAS, 315, 356
Horner D. J., Mushotzky R. F., Scharf C. A., 1999, ApJ, 520, 78 (HMS99)
Irwin J. A., Bregman J. N., Evrard A. E., 1999, ApJ, 519, 518
Kaiser N., 1991, ApJ, 383, 104
Knight P. A., Ponman T. J., 1997, MNRAS, 289, 955
Komatsu E., Seljak U., 2001, MNRAS, 327, 1353
Lloyd-Davies E. J., Ponman T. J., Cannon D. B., 2000, MNRAS, 315, 689
Lowenstein M., 2000, ApJ, 532, 17
Markevitch M., 1998, ApJ, 504, 27
Mathiesen B. F., Evrard A. E., 2001, ApJ, 546, 100 (ME01)
Mohr J. J., Mathiesen B., Evrard A. E., 1999, ApJ, 517, 627
Muanwong O., Thomas P. A., Kay S. T., Pearce F. R., Couchman H. M. P., 2001, MNRAS, 552, L27 (M2001)
Navarro J. F., Frenk C. S., White S. D. M., 1997, ApJ, 490, 493
Nevalainen J., Markevitch M., Forman W., 1999, ApJ, 526, 1
Nevalainen J., Markevitch M., Forman W., 2000, ApJ, 536, 73
Oegerle W. R., Cowie L., Davidsen A., Hu E., Hutchings J., Murphy E., Sembach K., Woodgate B., 2001, ApJ, 560, 187
Pearce F. R., Couchman H. M. P., 1997, New Astron., 2, 411
Pearce F. R., Thomas P. A., Couchman H. M. P., Edge A. C., 2000, MNRAS, 317, 1029
Peterson J. R., Ferrigno C., Kaastra J. S., Paerels F. B. S., Kahn S. M., Jernigan J. G., Bleeker J. A. M., Tamura T., 2002, in New Visions of the X-ray Universe in the XMM-Newton and Chandra Era, 2001 November. ESTEC, The Netherlands (astro-ph/0202108)
Ponman T. J., Bourner P. D. J., Ebeling H., Böhringer H., 1996, MNRAS, 283, 690
Ponman T. J., Cannon D. B., Navarro J. F., 1999, Nat, 397, 135
Raymond J. C., Smith B. W., 1977, ApJS, 35, 419
Roussel H., Sadat R., Blanchard A., 2000, A&A, 361, 429
Steinmetz M., White S. D. M., 1997, MNRAS, 288, 545
Sutherland R. S., Dopita M. A., 1993, ApJS, 88, 253
Thacker R. J., Couchman H. M. P., 2001, ApJ, 555, L17
Thomas P. A., Couchman H. M. P., 1992, MNRAS, 257, 11
Thomas P. A., Muanwong O., Pearce F. R., Couchman H. M. P., Edge A. C., Jenkins A., Onuora L., 2001, MNRAS, 324, 450 (T2001)
Thomas P. A., Muanwong O., Kay S. T., Liddle A. R., 2002, MNRAS, 330, L48
van Haarlem M. P., Frenk C. S., White S. D. M., 1997, MNRAS, 287, 817
Voit G. M., Bryan G. L., Balogh M. L., Bower R. G., 2002, ApJ, in press (astro-ph/020524)
White D. A., 2000, MNRAS, 312, 663
White D. A., Jones C., Forman W., 1997, MNRAS, 292, 419
White S. D. M., 1992, in Fabian A. C., ed., NATO ASI on Clusters and Superclusters of Galaxies. Kluwer, Dordrecht, p. 17
White S. D. M., Frenk C. S., 1991, ApJ, 379, 52
Wu K. K. S., Fabian A. C., Nulsen P. E. J., 2000, MNRAS, 318, 889
Wu X.-P., Xue Y.-J., 2002a, ApJ, 569, 112
Wu X.-P., Xue Y.-J., 2002b, ApJ, 572, L19
Xu H., Jin G., Wu X.-P., 2001, ApJ, 553, 78 (XJW01)
Xue Y.-J., Wu X.-P., 2000, ApJ, 538, 65

This paper has been typeset from a TEX/LATEX file prepared by the author.